

Cite this: *RSC Adv.*, 2018, 8, 3470



Received 14th December 2017

Accepted 11th January 2018

DOI: 10.1039/c7ra13336g

rsc.li/rsc-advances

# Reducing series resistance in $\text{Cu}_2\text{ZnSn}(\text{S},\text{Se})_4$ nanoparticle ink solar cells on flexible molybdenum foil substrates†

Xinya Xu,  Yongtao Qu, Vincent Barrioz, Guillaume Zoppi and Neil S. Beattie \*

Earth abundant  $\text{Cu}_2\text{ZnSnS}_4$  nanoparticle inks were deposited on molybdenum foil substrates and subsequently converted to high quality thin film  $\text{Cu}_2\text{ZnSn}(\text{S},\text{Se})_4$  photovoltaic absorbers. Integration of these absorbers within a thin film solar cell device structure yields a solar energy conversion efficiency which is comparable to identical devices processed on rigid glass substrates. Importantly, this is only achieved when a thin layer of molybdenum is first applied directly to the foil. The layer limits the formation of a thick  $\text{Mo}(\text{S},\text{Se})_x$  layer resulting in a substantially reduced series resistance.

## Introduction

$\text{Cu}_2\text{ZnSn}(\text{S},\text{Se})_4$  (CZTSSe) is considered a promising photovoltaic absorber material due to its high theoretical power conversion efficiency, ideal direct energy band-gap for solar light conversion and large absorption coefficient in the visible range.<sup>1,2</sup> Recently, Solar Frontier achieved a new world record  $\text{Cu}(\text{In},\text{Ga})\text{Se}_2$  (CIGS) thin-film solar cell efficiency of 22.9%,<sup>3</sup> however, it contains In and Ga, limiting its wide application. The related absorber material CZTS contains only earth-abundant elements and it is relatively low-cost, making it suitable for large area manufacture.<sup>4</sup> In addition, fabrication on flexible substrates has the potential to create lightweight solar cells that offer a wide range of application, such as roll-to-roll manufacturing and integration on a variety of surfaces including automotive and buildings. The high power-to-mass ratio of flexible solar cells further favour the applications on both space and ground utilities.<sup>5</sup> Inorganic photovoltaic technologies are generally recognized for their operational stability. In addition, nearly all of them require high temperature treatment during the fabrication and this is a particular advantage of using molybdenum foil as a substrate as it is compatible with the high temperatures (>500 °C) required to form large grains in a thin film photovoltaic absorber. CZTSSe solar cells on rigid glass substrates using hydrazine processing have achieved efficiency as high as 12.6%,<sup>6</sup> while CZTSSe solar cells based on less hazardous nanoparticle inks have also reached 9.3%.<sup>7</sup> However, research on  $\text{Cu}_2\text{ZnSnS}_4$  (CZTS) nanoparticle inks on flexible substrates is still comparatively limited with the highest

reported efficiency of 6.1% additionally with MoNa and Ge doping.<sup>8</sup>

There are several promising substrate candidates for flexible CZTS and CZTSSe solar cells including stainless steel<sup>8,9</sup> and glass.<sup>10</sup> In choosing a suitable flexible substrate, the coefficient of thermal expansion (CTE), surface smoothness, and chemical inertness should be taken consideration.<sup>11</sup> Molybdenum (Mo) foil has the advantage over polymers in that it is robust to high temperature processing however, in an important work, Zhang *et al.* report degradation of the device performance stemming from high series resistance ( $R_s$ ).<sup>12</sup>

Among the landscape of research on flexible substrates, there are currently no reports of CZTSSe solar cells on Mo foils. In this work we show that CZTSSe solar cells from CZTS nanoparticle inks can be fabricated directly on commercially available Mo foil substrates. Furthermore, we demonstrate that the origin of high  $R_s$  is a consequence of a thick  $\text{Mo}(\text{S},\text{Se})_x$  that forms between the foil substrate and the photovoltaic absorber. This can be overcome *via* the application of a thin sputtered Mo layer on the foil resulting in values of  $R_s$  which are the same as those for identical solar cells built on rigid glass substrates.

## Experimental details

Mo foil (99.9%, Sigma Aldrich) was chosen as the flexible substrate, due to its thermal stability and high conductivity. The CTE for molybdenum is approximately  $5.5 \times 10^{-6} \text{ K}^{-1}$  in the range 25–500 °C (ref. 13) which is slightly lower than the CTE for soda lime glass (SLG). The dimensions of the Mo foil substrate were cut to be 25 mm × 25 mm × 0.1 mm. The flexible substrates were prepared in two different ways: one was the bare Mo foil with corresponding resistivity of 5.0  $\mu\Omega \text{ cm}$ ; while the other was the Mo foil coated with an 800 nm thick Mo film with similar resistivity to bare Mo foil. Additionally, an SLG rigid substrate was used for comparison purposes with dimensions

Department of Mathematics, Physics and Electrical Engineering, Northumbria University, Newcastle-upon-Tyne, NE1 8ST, UK. E-mail: neil.beattie@northumbria.ac.uk

† Electronic supplementary information (ESI) available. See DOI: 10.1039/c7ra13336g



25 mm × 25 mm × 1 mm and coated with a 800 nm thick Mo film with resistivity of 50.7  $\mu\Omega$  cm.

The Mo films on SLG and Mo film were sputtered by direct current magnetron sputtering with target power density of 9 mW cm<sup>-2</sup> and argon pressure of 7 mTorr at room temperature. Surface roughness ( $R_a$ ) of the substrates as measured by atomic force microscope (AFM) were 3.30 nm, 3.15 nm and 2.18 nm for foil, foil with sputtered Mo film and Mo coated glass substrates, respectively (see Fig. S1 in the ESI†).

Solar cell devices fabricated on these substrates had the following structure: substrate/(Mo film)/CZTSSe/CdS/ZnO/ITO/Ni/Al, where ITO denotes indium tin oxide. Initially, CZTS nanoparticles were fabricated by injection of metallic precursors into a hot surfactant as described in ESI (S1†) and reported elsewhere.<sup>14</sup> All substrates were initially cleaned in deionized water and isopropanol for 15 min in ultrasonic bath. Additionally, the bare Mo foil substrate was oxygen plasma cleaned for 5 min to remove any organic contaminants and surface oxide. To fabricate the photovoltaic absorber, CZTS nanoparticle inks were spin-coated on the substrates 10 times to obtain a precursor film thickness of 1.5  $\mu$ m (Fig. S2†).<sup>15</sup> The CZTS precursor films were found to be uniform from SEM and AFM analyses (Fig. S3†). No obvious difference was observed between the samples prepared on foil, foil with sputtered Mo and glass. The precursor films were then selenised in a tube furnace under a selenium atmosphere for 20 min at 500 °C to form the CZTSSe absorber layers. The solar cell structures were completed by subsequently depositing a thin CdS layer by chemical bath deposition and a bilayer intrinsic ZnO/ITO layer by magnetron sputtering. Finally, a Ni/Al front contact grid was deposited by electron beam evaporation through a shadow mask. Each substrate was mechanically scribed to define nine 0.16 cm<sup>2</sup> individual devices.

AFM (Veeco Dimension-3100) and scanning electron microscopy (SEM, Tescan Mira 3) were used to investigate the surface morphology and cross-sectional structure. Energy dispersive spectroscopy (EDS) attached to the SEM was used to determine the elemental composition and X-ray diffraction (XRD, Siemens D-5000) using a CuK $\alpha$  radiation source ( $\lambda$  = 0.154 nm for K $\alpha_1$ ) was used to assess the crystal structure. Raman spectroscopy with a Horiba Labram HR system was used to capture the Raman shift with 632.8 nm excitation. Secondary ion mass spectroscopy (SIMS) using a Hiden Analytical gas ion gun and quadrupole detector was used to obtain the depth profile. Photocurrent density–voltage characteristic of the CZTSSe solar cells were measured under a standard air mass 1.5 solar illumination with an intensity of 100 mW cm<sup>-2</sup> (Abet Technologies Sun 2000 Solar Simulator). External quantum efficiency (EQE) measurements were performed using a double grating monochromator with illumination normalized against calibrated silicon and germanium detectors.

## Results and discussion

### Structural characterisation

Fig. 1a shows the XRD spectra of CZTSSe thin films fabricated on the three substrates (SLG, Mo foil, Mo foil + Mo). Major

peaks at 27.34°, 45.35° and 53.7° can be indexed as (112), (204) and (312) planes corresponding to the Cu<sub>2</sub>ZnSnSe<sub>4</sub> structure (PDF no. 01-070-8930), suggesting that the films are polycrystalline with kesterite crystal structure. From the position of the (112) peaks on all three substrates, the observed inter-planar spacing  $d$  values approach the standard  $d$  value of 3.28 Å. The precise peak positions in the XRD spectra are affected by the relative ratio of Se and S: increasing Se content causes a shift to lower  $2\theta$  angles as a result of its larger atomic radius (~0.198 nm) compared to sulphur (~0.184 nm).<sup>16</sup> Since the three samples show very close peak positions and match well with standard Cu<sub>2</sub>ZnSnSe<sub>4</sub> patterns, the samples can be considered highly selenized with only a very small amount of residual S.

The texture coefficients ( $C_{hkl}$ ) and preferred orientation were calculated as described in ESI (S2†).<sup>17</sup> As shown in Table S1 and Fig. S4,† the  $C_{hkl}$  values increase for minor reflections (101), (211) and (400) for film deposited directly on Mo foil. While this would indicate a small randomisation of the sample texturing compared to film/foil and film/glass substrate, the absence of reflections at (110) and (332) points toward a slight preferred orientation (increase in  $\sigma$  value) along the minor planes.

In addition to the CZTSSe reflections, the Mo film on glass substrate shows mainly the (110) orientation while the bare Mo

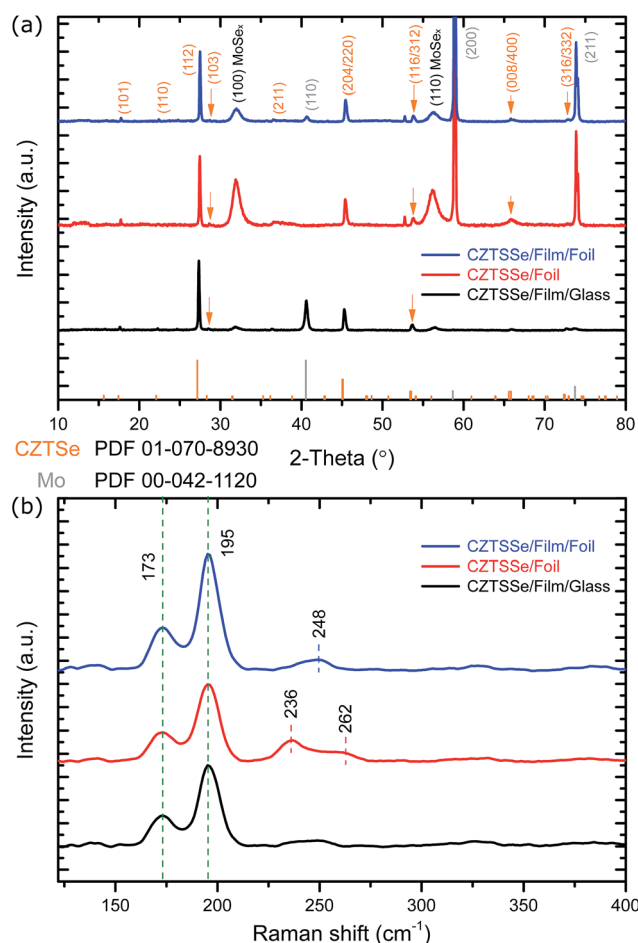


Fig. 1 (a) XRD patterns and (b) Raman scattering spectra of absorber samples on different substrates.



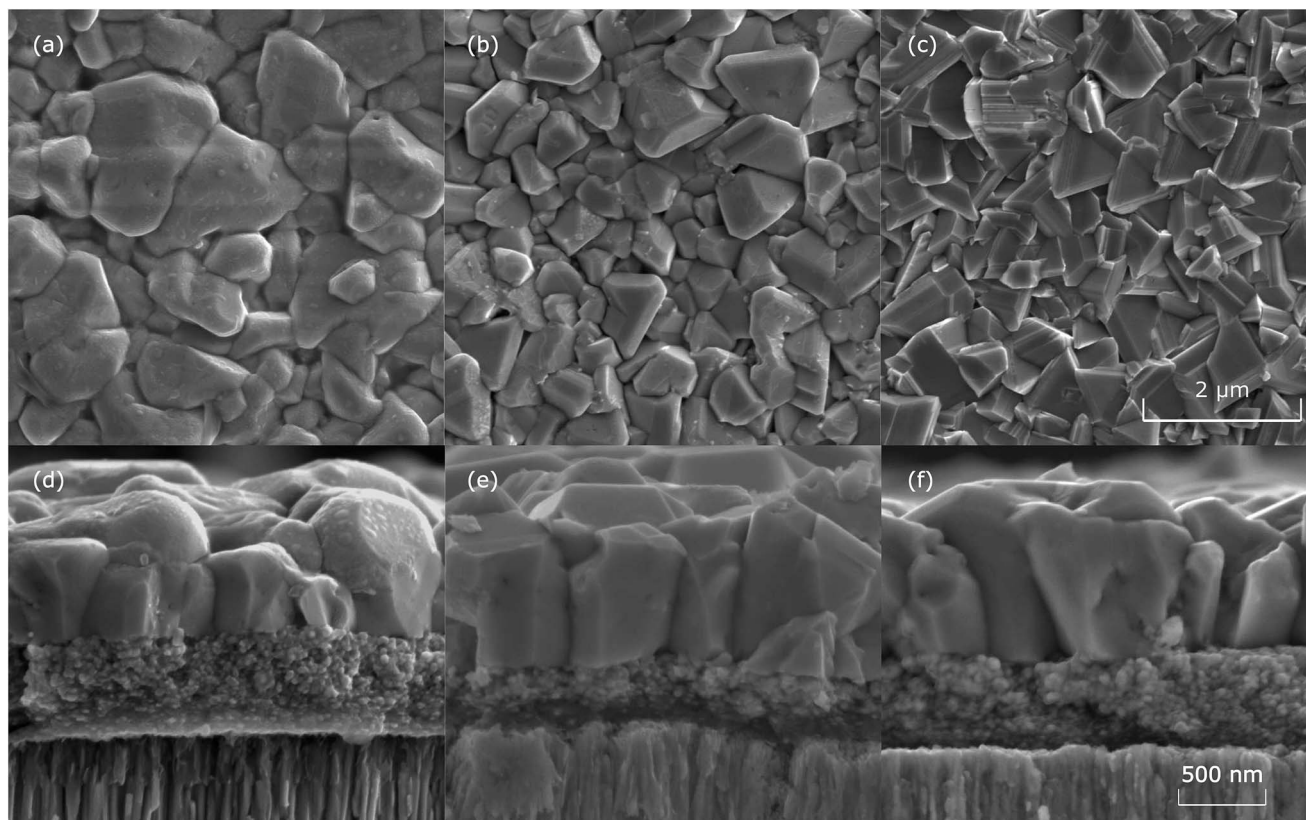


Fig. 2 Surface morphology of CZTSSe sample on (a) SLG, (b) molybdenum foil and (c) molybdenum foil with Mo film. Cross-sectional image of samples on (d) SLG, (e) molybdenum foil and (f) molybdenum foil with Mo film.

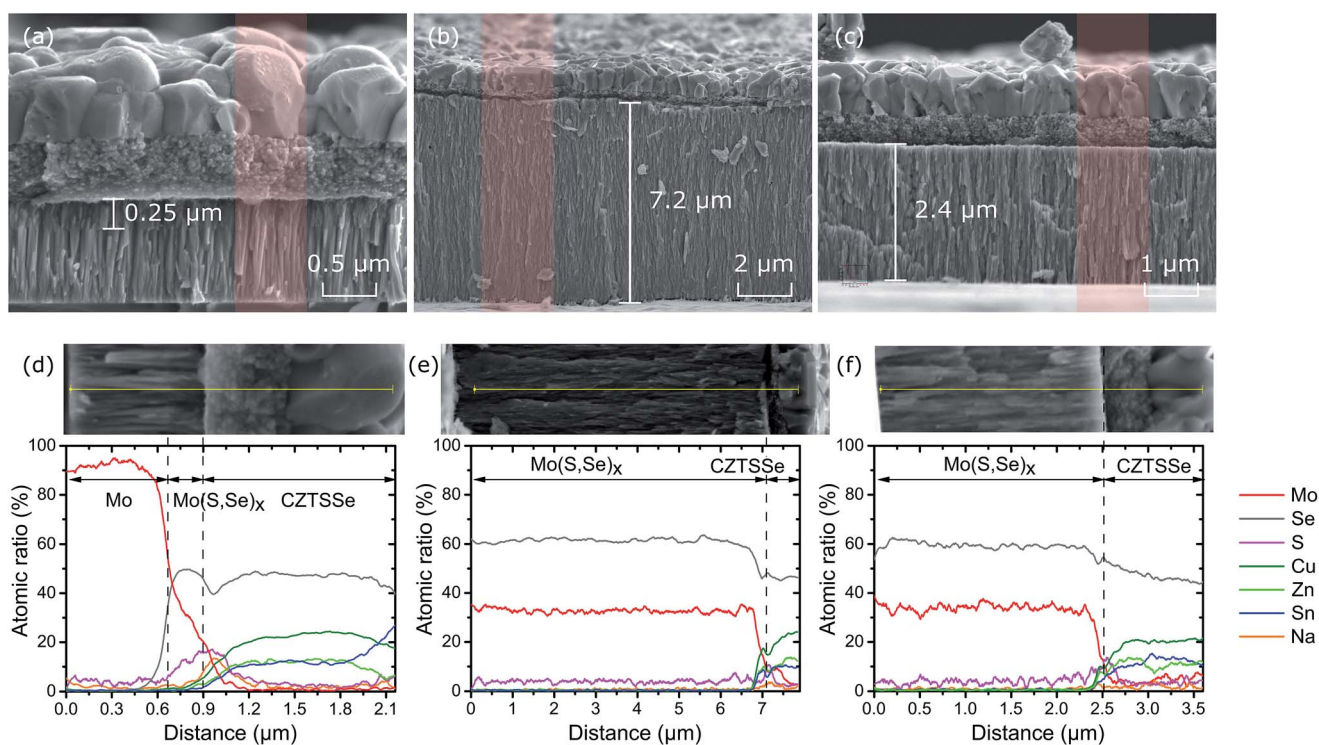


Fig. 3 The full range cross-sectional SEM images for samples on (a) SLG, (b) molybdenum foil and (c) molybdenum foil with Mo film layer, and EDS line scans across the film thickness in (d), (e) and (f), respectively. The red regions show the positions of EDS line scans.





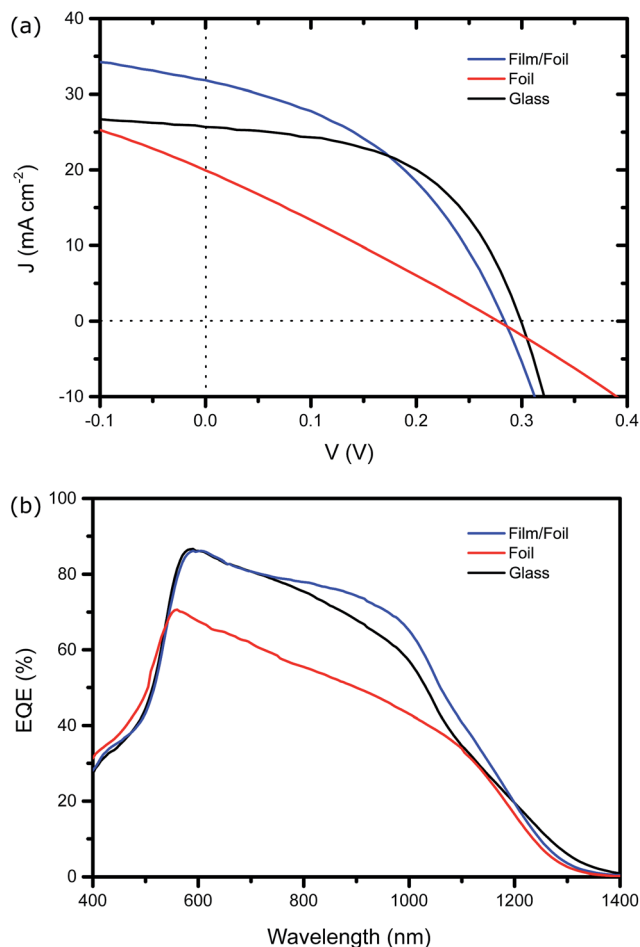


Fig. 4 (a) JV curves and (b) EQE response of solar cells on rigid and flexible substrates.

foil shows both the (200) and (211) orientations. Sputtered Mo on Mo foil shows all three diffraction planes (Fig. S5†). Despite these different orientations,  $\text{Mo}(\text{S,Se})_x$  is found on all three substrates at  $31.9^\circ$  and  $56.3^\circ$  corresponding to (100) and (110) planes following selenisation.<sup>18</sup> In this case the  $\text{Mo}(\text{S,Se})_x$  grains are oriented perpendicular to the Mo substrate increasing the adhesion and the electrical conductivity<sup>19</sup> but also facilitating the diffusion of Se, leading to a thicker  $\text{Mo}(\text{S,Se})_x$  layer.<sup>20</sup> Interestingly, the strength of the  $\text{Mo}(\text{S,Se})_x$  peaks of samples on foil with sputtered Mo are weaker than those on bare foil. This suggests that the sputtered Mo has limited the formation of  $\text{Mo}(\text{S,Se})_x$  on this substrate.

The XRD results alone cannot conclusively confirm the crystal structure because of the peak positions for kesterite and stannite CZTSSe are the same as well as secondary phases such

as ZnSe and  $\text{Cu}_2\text{SnSe}_3$ .<sup>21,22</sup> Therefore, Raman spectroscopy was performed and, as shown in Fig. 1b, there is a dominant  $A_1$  symmetry mode of CZTSSe at  $173\text{ cm}^{-1}$  and  $195\text{ cm}^{-1}$ .<sup>23</sup> The presence of Raman peaks in the region of  $236\text{--}248\text{ cm}^{-1}$  for the films on flexible foils can correspond to a mix mode of B/E<sup>24</sup> modes.

### Morphology and composition

Fig. 2 shows representative morphology of the samples on each substrate. For the reference sample on SLG, shown in Fig. 2a, the CZTSSe film has compact and rounded grains with a size of  $1\text{--}2\text{ }\mu\text{m}$  forming a dense thin film. For the CZTSSe films on Mo foil shown in Fig. 2b and c, the grains are smaller with a size of  $0.8\text{--}1.2\text{ }\mu\text{m}$ . This reduction in grain size is likely to stem from the absence of Na doping which is introduced by the SLG substrate. All three cross-sectional images (Fig. 2d–f) exhibit a characteristic bi-layer morphology associated the CZTS nanoparticle ink fabrication approach, *i.e.* a large grain layer on top of a fine-grain (FG) layer located between the CZTSSe layer and Mo back contact. The thickness of the large-grain (LG) CZTSSe layer was similar for all of the samples at around  $750\text{ nm}$ . This is reasonable given that the same selenisation conditions were applied (selenium mass, temperature and time). We have previously reported that the selenisation process is controlled by metal cation re-ordering and grain boundary migration.<sup>25</sup>

As shown in Fig. 3a, the full range cross-sectional image of CZTSSe on SLG, a thin  $250\text{ nm}$   $\text{Mo}(\text{S,Se})_x$  layer is formed between the CZTSSe absorber and Mo back contact during selenisation. This is similar for widely reported CZTSSe solar cells.<sup>26,27</sup> On the other hand, for samples on Mo foil substrates (Fig. 3b and c), the  $\text{Mo}(\text{S,Se})_x$  layer was much thicker than that on SLG. This is especially true for the  $\text{Mo}(\text{S,Se})_x$  layer on bare Mo foil which was up to  $7.2\text{ }\mu\text{m}$ . The application of a sputtered Mo film on Mo foil substrate reduced this to  $2.4\text{ }\mu\text{m}$ . This difference between the samples is consistent with the trend observed in the XRD spectra for  $\text{Mo}(\text{S,Se})_x$ . The thicknesses of the  $\text{Mo}(\text{S,Se})_x$  layers were further confirmed with EDS line scans (Fig. 3d–f) corresponding to the red regions marked in Fig. 3a–c. It can be seen clearly from Fig. 3e and f that the layer between the flexible foil back contact and CZTSSe absorber consists mainly of Mo and Se in the atomic ratio of around  $1 : 2$ . For the sample on SLG (Fig. 3a), the  $\text{Mo}(\text{S,Se})_x$  formed only a thin layer on top of Mo film back contact.

### Photovoltaic current–voltage characteristics

Thin film solar cells were fabricated on all three substrates and the current density ( $J$ ) versus voltage ( $V$ ) characteristics for

Table 1 Optoelectronic parameters of CZTSSe solar cells on different substrate

Substrate	$V_{OC}$ (mV)	$J_{SC}$ ( $\text{mA cm}^{-2}$ )	FF (%)	PCE (%)	$R_s$ ( $\Omega\text{ cm}^2$ )	$R_{sh}$ ( $\Omega\text{ cm}^2$ )
Mo foil	280 ( $247 \pm 7.0$ )	19.9 ( $19.6 \pm 1.9$ )	27.3 ( $27.8 \pm 0.4$ )	1.5 ( $1.35 \pm 0.17$ )	12.2	16.7
Mo foil + film	280 ( $276 \pm 9.6$ )	31.8 ( $28.4 \pm 3.8$ )	42.6 ( $45.0 \pm 2.4$ )	3.8 ( $3.48 \pm 0.24$ )	2.9	36.3
Glass	300 ( $302 \pm 7.8$ )	25.7 ( $25.6 \pm 0.8$ )	53.8 ( $49.5 \pm 2.4$ )	4.0 ( $3.8 \pm 0.19$ )	2.5	72.8



champion devices are shown in Fig. 4a. The extracted photovoltaic performance characteristics together with average performance values are listed in Table 1. It can be seen that the device on SLG exhibited a power conversion efficiency (PCE) of 4.0% while in contrast the device on bare flexible Mo had a PCE of 1.5%. Despite achieving a similar  $V_{OC}$ , the degradation can be attributed to a substantially increased series resistance  $R_s$  caused by the existence of the thick  $\text{Mo}(\text{S,Se})_x$  layer. The effect of the sputtered Mo layer is immediately clear in Fig. 4a as the PCE becomes comparable to the SLG device at 3.8%. Notably, the power density achieved with the flexible cell is more than double that of the device on SLG. From Table 1, it can be seen that while the flexible device achieves a similar value of  $R_s$  using a sputtered Mo layer,  $R_{sh}$  is significantly lower than the device on SLG. This is attributed to the increased grain boundary density in the CZTSSe absorber on foil substrates. For the Mo foil with sputtered Mo film device presented in Fig. 4a and Table 1, the thickness of the sputtered Mo layer was approximately 800 nm. Increasing this to 1200 nm further reduced this to  $2.6 \Omega \text{ cm}^2$ , confirming the hypothesis that limiting the formation of the  $\text{Mo}(\text{S,Se})_x$  layer reduces series resistance.

Fig. 4b shows the EQE characteristics for the three devices. The signal for the device on bare foil is substantially reduced relative to the SLG and foil with sputtered Mo substrates. This is due to the vastly reduced collection probability created by a performance limiting  $\text{Mo}(\text{S,Se})_x$  layer. Interestingly, the EQE for the device on foil with sputtered Mo has a slightly larger EQE towards long wavelengths despite having smaller average grain size. This is consistent with the values of  $J_{SC}$  obtained from Fig. 4a (and listed in Table 1) and suggests considerable potential for the technology.

### Investigation of substrate impurities

In order to assess the quality of the Mo foil substrate onto which the CZTS nanoparticle inks were deposited, SIMS measurements were performed on the bare Mo foil and the Mo foil with

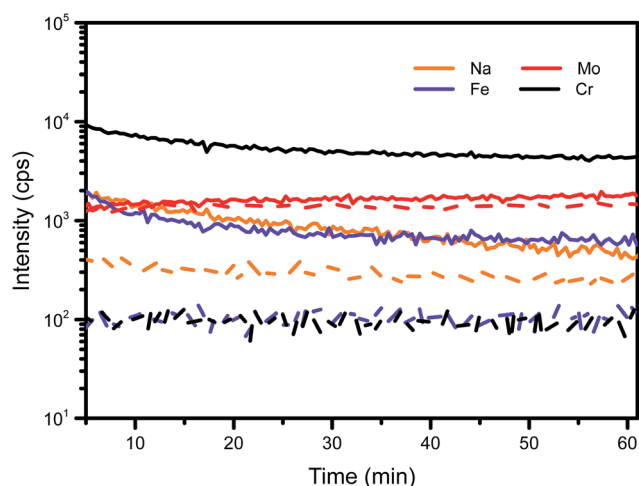


Fig. 5 SIMS elemental depth profiles of Mo foil substrate (solid lines) and Mo foil coated with Mo film substrate (dash lines).

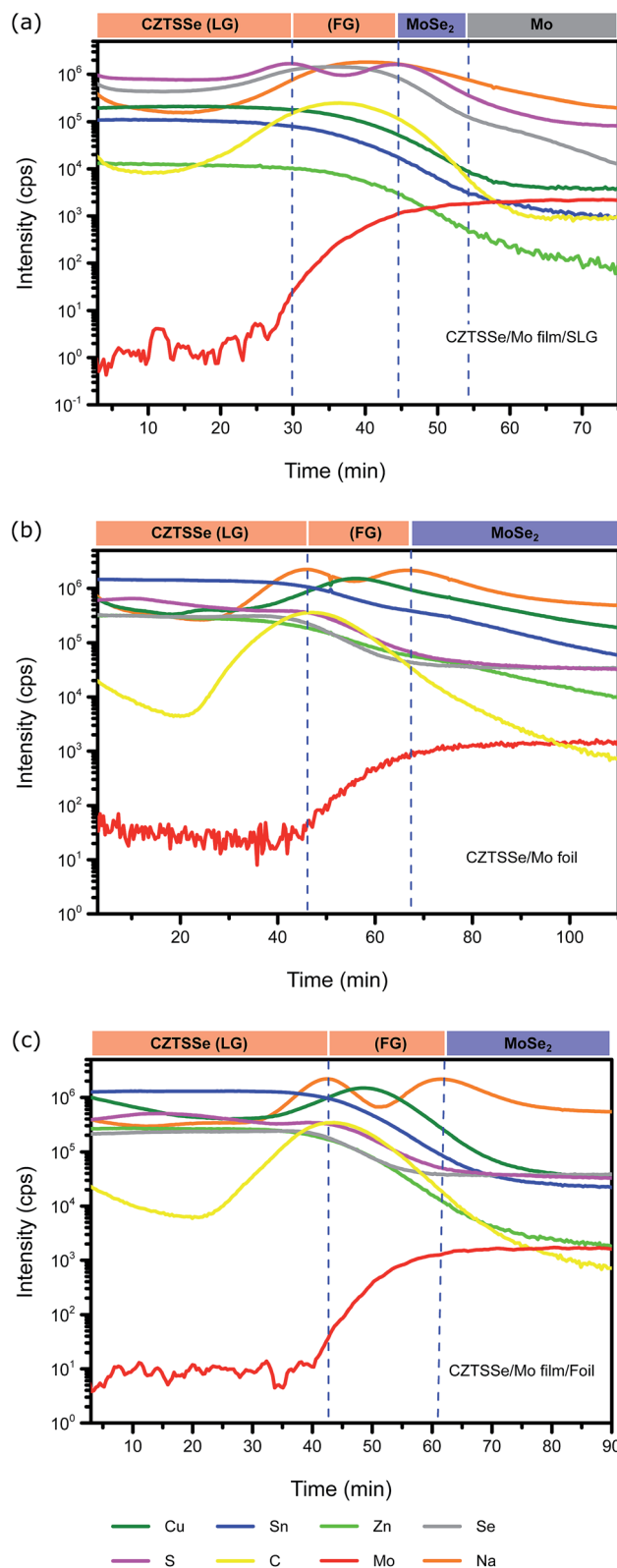


Fig. 6 SIMS elemental depth profiles of CZTSSe on substrate (a) SLG, (b) molybdenum foil, and (c) molybdenum foil with Mo film layer. LG: larger-grain, FG: fine-grain.



a sputtered thin Mo film. These data are shown in Fig. 5, the bare foil substrate exhibits one and two orders of magnitude higher levels of Fe and Cr respectively, than the Mo foil with Mo film. Note that in the case of the Mo foil coated with Mo film, the ion beam has not penetrated through the sputtered Mo layer to the foil. As expected therefore, the sputtered Mo provides a purer substrate than the bare foil and may result in a better interface within the device. It can be concluded that on its own Mo foil is unsuitable as a substrate for flexible CZTSSe solar cells.

Fig. 5 also indicates a difference in Na signal between the substrates which, although not as large as for Fe and Cr, is still significant. The influence of sodium incorporation on CZTSSe morphology and cell performances have been widely reported<sup>8,9,28–31</sup> and it plays a positive role in the reduction of grain boundary density *via* the formation of large grains. The use of SLG as a rigid substrate in our work provides an intentional source of intrinsic Na doping. However, using Mo foil as a substrate unintentionally introduces Na into our process.

In addition to the Mo foil, background sources of Na may also exist in the process arising for example from the selenisation furnace.<sup>20</sup> In order to assess the possible influence of these, elemental depth profiling was performed on devices built on all three substrates using SIMS as shown in Fig. 6. The SIMS data allow for identification of the various layers in the devices including the Mo(S,Se)<sub>x</sub> and FG/LG CZTSSe layers. All three samples exhibit an oscillating Na signal throughout the device which confirms the presence of uncontrolled Na sodium sources in the fabrication process. Interestingly, the device on SLG shows a local maximum in the Na signal in the FG CZTSSe layer (Fig. 6a) while in contrast the devices on foil show a local minima in the same region. This reduction may be responsible for the smaller average grain size observed in the LG CZTSSe layer in the foil devices and overall, these features merit further investigation to achieve comparable  $R_{sh}$  in Mo foil devices.

## Conclusions

The performance of thin film CZTSSe solar cells fabricated on Mo foil substrates has been presented. It is found that on its own, Mo foil is an unsuitable substrate due to the formation of a thick Mo(S,Se)<sub>x</sub> layer formed during the fabrication. These effects can be mitigated by the introduction of a thin Mo sputtered layer which preserves the advantages of a low cost foil substrate that is compatible with high volume manufacturing. Devices on SLG contain an intrinsic source of Na doping which promotes the formation of large grains in the CZTSSe photovoltaic absorber. For development of the technology on foil substrates, it is necessary to develop approaches towards controlled introduction of Na, also achieve comparable grain sizes and  $R_{sh}$  to SLG.

## Conflicts of interest

There are no conflicts to declare.

## Acknowledgements

The authors gratefully acknowledge financial support for this work from the Engineering and Physical Sciences Research Council *via* grants: the North East Centre for Energy Materials (EP/N024389/1) and EP/R021503/1. We would also like to acknowledge useful interactions with Patrick Chapon (Horiba) and Kate Nicholson (Northumbria University).

## References

- 1 X. Liu, Y. Feng, H. Cui, F. Liu, X. Hao, G. Conibeer, D. B. Mitzi and M. Green, *Prog. Photovoltaics*, 2016, **24**, 879–898.
- 2 F. Luckert, D. I. Hamilton, M. V. Yakushev, N. S. Beattie, G. Zoppi, M. Moynihan, I. Forbes, A. V. Karotki, A. V. Mudryi, M. Grossberg, J. Krustok and R. W. Martin, *Appl. Phys. Lett.*, 2011, **99**, 062104.
- 3 S. Yoshida, *Solar Frontier Achieves World Record Thin-Film Solar Cell Efficiency of 22.9%*, 2017, [http://www.solar-frontier.com/eng/news/2017/1220\\_press.html](http://www.solar-frontier.com/eng/news/2017/1220_press.html).
- 4 H. Zhou, W.-C. Hsu, H.-S. Duan, B. Bob, W. Yang, T.-B. Song, C.-J. Hsu and Y. Yang, *Energy Environ. Sci.*, 2013, **6**, 2822–2838.
- 5 N. G. Dhere, *Sol. Energy Mater. Sol. Cells*, 2007, **91**, 1376–1382.
- 6 W. Wang, M. T. Winkler, O. Gunawan, T. Gokmen, T. K. Todorov, Y. Zhu and D. B. Mitzi, *Adv. Energy Mater.*, 2014, **4**, 1301465.
- 7 C. J. Hages, M. J. Koeper, C. K. Miskin, K. W. Brew and R. Agrawal, *Chem. Mater.*, 2016, **28**, 7703–7714.
- 8 S. Lopez-Marino, Y. Sanchez, M. Espindola-Rodriguez, X. Alcobe, H. Xie, M. Neuschitzer, I. Becerril, S. Giraldo, M. Dimitrievska, M. Placidi, L. Fourdrinier, V. Izquierdo-Roca, A. Perez-Rodriguez and E. Saucedo, *J. Mater. Chem. A*, 2016, **4**, 1895–1907.
- 9 K. Sun, F. Liu, C. Yan, F. Zhou, J. Huang, Y. Shen, R. Liu and X. Hao, *Sol. Energy Mater. Sol. Cells*, 2016, **157**, 565–571.
- 10 K. W. Brew, S. M. McLeod, S. M. Garner and R. Agrawal, *Thin Solid Films*, 2017, **642**, 110–116.
- 11 P. Reinhard, A. Chirilă, P. Blösch, F. Pianezzi, S. Nishiwaki, S. Buecheler and A. N. Tiwari, *IEEE J. Photovolt.*, 2013, **3**, 572–580.
- 12 Y. Zhang, Q. Ye, J. Liu, H. Chen, X. He, C. Liao, J. Han, H. Wang, J. Mei and W. Lau, *RSC Adv.*, 2014, **4**, 23666–23669.
- 13 P. Hidnert, W. B. Gero and S. United, *Thermal expansion of molybdenum*, U.S. Dept. of Commerce, Bureau of Standards: U.S. Govt. Print. Off., Washington, D.C., 1924, vol. 19, pp. 429–444.
- 14 Y. Qu, G. Zoppi, R. W. Miles and N. S. Beattie, *Mater. Res. Express*, 2014, **1**, 045040.
- 15 M. A. Baker, *Thin Solid Films*, 1980, **69**, 359–368.
- 16 S. C. Riha, B. A. Parkinson and A. L. Prieto, *J. Am. Chem. Soc.*, 2011, **133**, 15272–15275.
- 17 G. Zoppi, K. Durose, S. Irvine and V. Barrioz, *Semicond. Sci. Technol.*, 2006, **21**, 763.
- 18 P. B. James and M. T. Lavik, *Acta Crystallogr.*, 1963, **16**, 1183.



- 19 R. Würz, D. Fuertes Marrón, A. Meeder, A. Rumberg, S. M. Babu, T. Schedel-Niedrig, U. Bloeck, P. Schubert-Bischoff and M. C. Lux-Steiner, *Thin Solid Films*, 2003, **431**, 398–402.
- 20 D. Abou-Ras, D. Mukherji, G. Kostorz, D. Brémaud, M. Kälin, D. Rudmann, M. Döbeli and A. N. Tiwari, *MRS Online Proc. Libr.*, 2005, **865**, 1946–4274.
- 21 B. Ananthoju, J. Mohapatra, M. K. Jangid, D. Bahadur, N. V. Medhekar and M. Aslam, *Sci. Rep.*, 2016, **6**, 35369.
- 22 P. A. Fernandes, P. M. P. Salomé and A. F. da Cunha, *J. Alloys Compd.*, 2011, **509**, 7600–7606.
- 23 P. M. P. Salomé, P. A. Fernandes and A. F. da Cunha, *Thin Solid Films*, 2009, **517**, 2531–2534.
- 24 M. A. Hossain, M. Wang and K.-L. Choy, *ACS Appl. Mater. Interfaces*, 2015, **7**, 22497–22503.
- 25 Y. Qu, G. Zoppi and N. S. Beattie, *Sol. Energy Mater. Sol. Cells*, 2016, **158**, 130–137.
- 26 C. K. Misken, W.-C. Yang, C. J. Hages, N. J. Carter, C. S. Joglekar, E. A. Stach and R. Agrawal, *Prog. Photovoltaics*, 2015, **23**, 654–659.
- 27 Y. Qu, G. Zoppi and N. S. Beattie, *Prog. Photovoltaics*, 2016, **24**, 836–845.
- 28 D. Colombara, U. Berner, A. Ciccioli, J. C. Malaquias, T. Bertram, A. Crossay, M. Schöneich, H. J. Meadows, D. Regesch, S. Delsante, G. Gigli, N. Valle, J. Guillot, B. El Adib, P. Grysan and P. J. Dale, *Sci. Rep.*, 2017, **7**, 43266.
- 29 H. A. Al-Thani, F. S. Hasoon, M. Young, S. Asher, J. L. Alleman, M. M. Al-Jassim and D. L. Williamson, *29th IEEE PVSC*, Research Org., National Renewable Energy Lab., Golden, CO, US, 2002.
- 30 J. V. Li, D. Kuciauskas, M. R. Young and I. L. Repins, *Appl. Phys. Lett.*, 2013, **102**, 163905.
- 31 H. Zhou, T.-B. Song, W.-C. Hsu, S. Luo, S. Ye, H.-S. Duan, C.-J. Hsu, W. Yang and Y. Yang, *J. Am. Chem. Soc.*, 2013, **135**, 15998–16001.

